Karlsruhe Institute of Technology

Interpretation of irregular water profiles at silica surfaces

Claudia Bucharsky, Günter Schell, Theo Fett

KIT SCIENTIFIC WORKING PAPERS 214

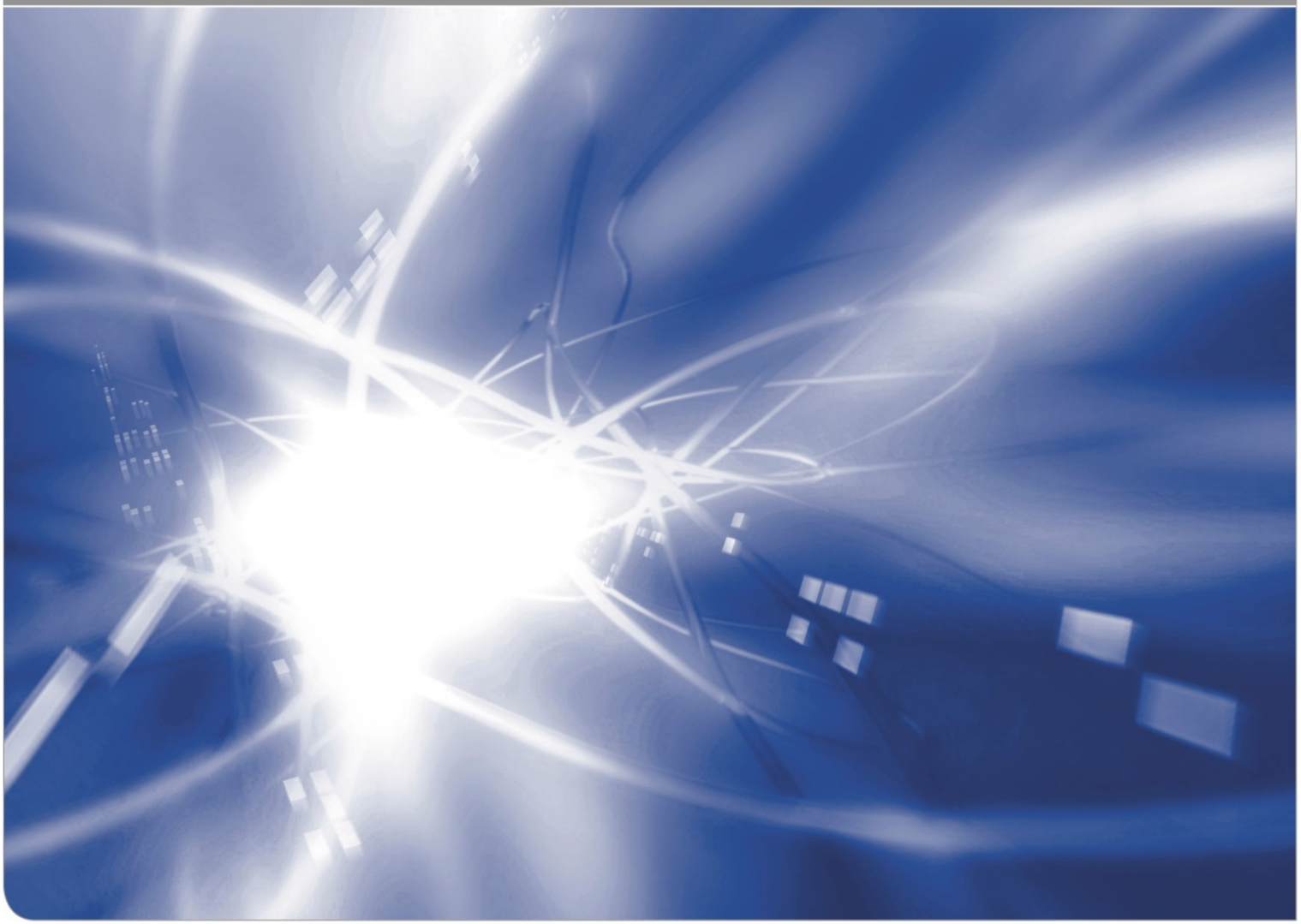

Institute for Applied Materials

Impressum

Karlsruher Institut für Technologie (KIT)
www.kit.edu

2023

ISSN: 2194-1629

Abstract

In the present Report, we will discuss the irregular water distributions at silica surfaces as were reported by the measured data from Zouine et al. [1], especially those at room temperature. The question was whether the deviations from the usually found erfc-shaped water profiles can be understood by competing diffusion and surface dissolution and whether back-diffusion after water or air storage, may affect the type of water profile.

We will come to the conclusion that the irregular distributions of the measured data by Zouine et al. [1], especially those at room temperature, can be understood by back-diffusion after water or air storage, respectively.

Contents

1 Irregular profiles

Water profiles in silica surfaces are mostly described by

$$C_w = C_w(0)\,\mathrm{erfc}\left(\frac{z}{2b}\right) \tag{1}$$

where erfc is the complementary error function. This profile is exact for the case that the surface concentration $C_w(0)=C_0$ is instantaneously present already at $t=0$. This profile is very often assumed in the treatment of diffusion problems and should therefore be referred to here as a "regular profile". The present report is intended to evaluate a much more complicated water diffusion profile. Water concentrations at silica surfaces under saturation pressure are available from an investigation by Zouine et al. [1].

Deviations from eq.(1), further referred to as irregular profiles, are not rare. Some examples for silica in humid environment are:

1. Diffusion under a limited mass transfer coefficient at the surface of silica [2,3],
2. diffusion coefficients, variable with respect to time or location ([4],[5]),
3. presence of a Beilby surface layer [6],
4. water profile modified by swelling stresses [7],
5. back-diffusion after water soaking [8],
6. moving surface by chemical water reaction [9,10].

In this report, we discuss especially irregular water distributions according to items 5 and 6.

Water concentrations at silica surfaces under saturation pressure are available from an investigation by Zouine et al. [1]. Some results in [1] deviate from the simple erfc-description as can be seen for measurements compiled in Fig. 1a. Figure 1b represents the same results in a normalized representation where $C(0)$ are the surface concentrations from Table 1 in [1] and additionally the concentrations are divided by the diffusion depth b at which the erfc function has the value of ≅½.

The irregular distributions of the measurement data from Zouine et al. [1], especially those at room temperature, can be understood by back-diffusion after water or air storage, respectively. Unfortunately, no detailed information on storage after the end of the experiment is given in [1]. It therefore remains unclear in which medium and for how long the samples were in until the subsequent NRA measurement. Due to this circumstance, only the possibility of the effect should be addressed here, but no quantitative information should be given.

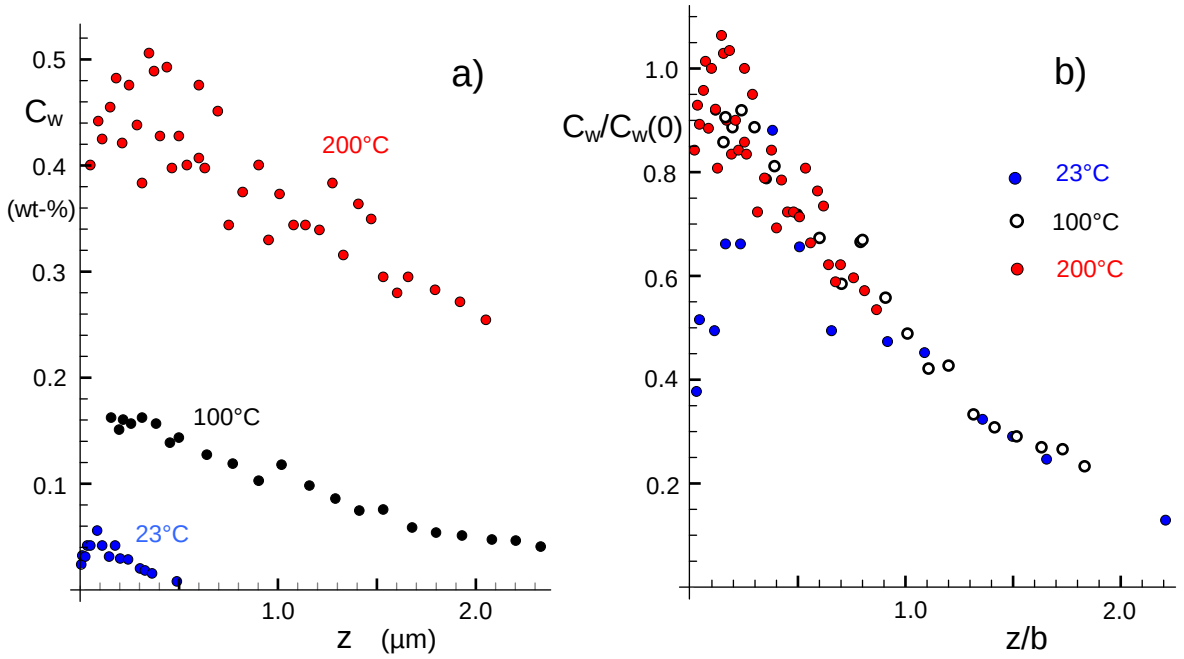

Fig. 1 Some irregular profiles a) total water content $C_w(z)$ measured by Zouine et al. [1], b) same data in normalized representation, with $C_w(0)=C_w(z=0)$.

This may be illustrated here by superimposing two erfc distributions of the type

$$C_w = a_0\,\mathrm{erfc}[a_1 z] + a_2\,\mathrm{erfc}[a_3 z] \tag{2}$$

or according to (1)

$$C_w = a_0\,\mathrm{erfc}[z/(2b_1)] + a_2\,\mathrm{erfc}[a_3 z] \tag{3}$$

the first describing diffusion during aging in the wet medium and the second describing diffusion towards the surface after aging. Zouine et al. [1] fitted the data far from the surface and thereby obtained the parameters a_0 and a_1 (introduced as curves in the original plots). Table 1 compiles these coefficients in the columns 2 and 3. Column 4 gives the diffusion length b_1 for the representation by eq.(3), i.e. $b_1=1/(2a_1)$.

We fitted the whole data by eq.(2) and obtained the two parameters a_2 and a_3, given in columns 5 and 6. The negative parameter a_1 can be taken as an indication of a reversal of diffusion. The best fitting curves are plotted in Figs. 2a-2c.

Temperature	a_0	a_1 (µm^{-1})	b_1 (µm)	a_2	a_3 (µm^{-1})
200°C	0.0052	0.2421	2.07	-0.00143	4.53
100°C	0.00177	0.377	1.33	-0.000254	5.73
23°C	0.00063	2.218	0.225	-0.00041	15.6

Table 1 Parameters for eq.(2) obtained by curve fitting to data of Figs. 2a-2c.

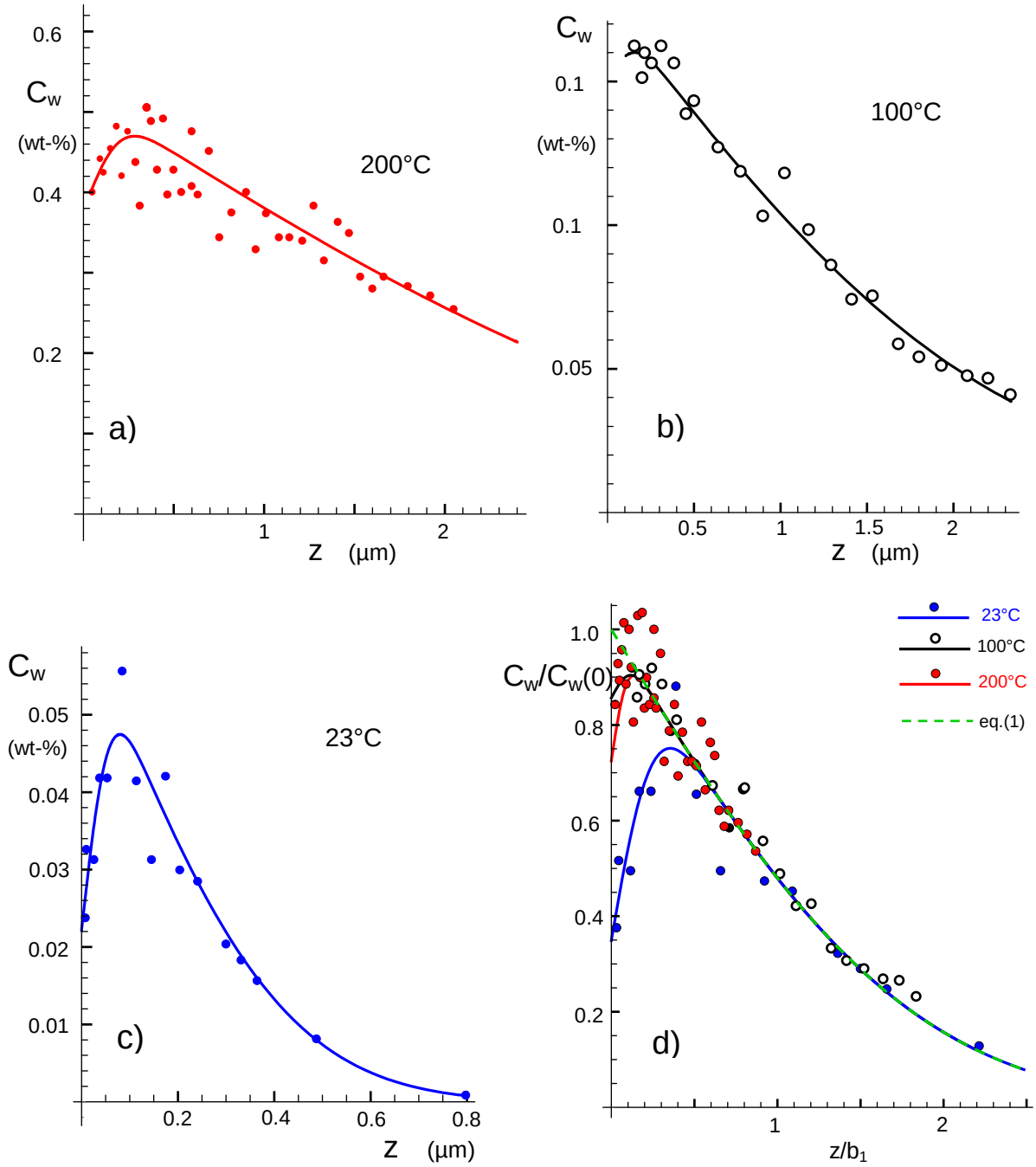

Fig. 2 a)-c) Total water profiles $C_w(z)$ for 3 temperatures, fitted by two superimposed erfc-functions according to eq.(2) using the parameters of Table 1; d) the individual profiles for 200°C, 100°C and 23°C in normalized representation.

2 Computation of water profiles

2.1 Equation for back diffusion

In [8], it was assumed that the decreases in concentration found at the surface could be a form of back diffusion or outgassing. This hypothesis is to be tested with regard to the expected shape of the water profiles. Due to the equivalence between diffusion and

heat conduction (interpreted as diffusion of phonons), the diffusion problem can be traced back to the heat conduction problem. A plate of thickness L is considered as plotted in Fig. 3. The origin of the z-coordinate, z=0, is at the left side.

The heat entrance into a plate by heat radiation may cause after a time t a symmetrical temperature distribution from both sides, illustrated by the red curves in Fig. 3a. The temperature T as a function of the coordinate z can be described by

$$T = T_0\left[\operatorname{erfc}\frac{z}{2b} + \operatorname{erfc}\frac{L-z}{2b}\right], \quad b/L \to 0 \tag{4}$$

where

$$b = \sqrt{\kappa t} \tag{5}$$

In the numerical computations we will consider the case $b/L \leq 0.025$. The parameter κ is the thermal diffusivity, defined by thermal conductivity λ, density ρ, and specific heat C_p at constant pressure:

.

$$\kappa = \frac{\lambda}{\rho C_p} \tag{6}$$

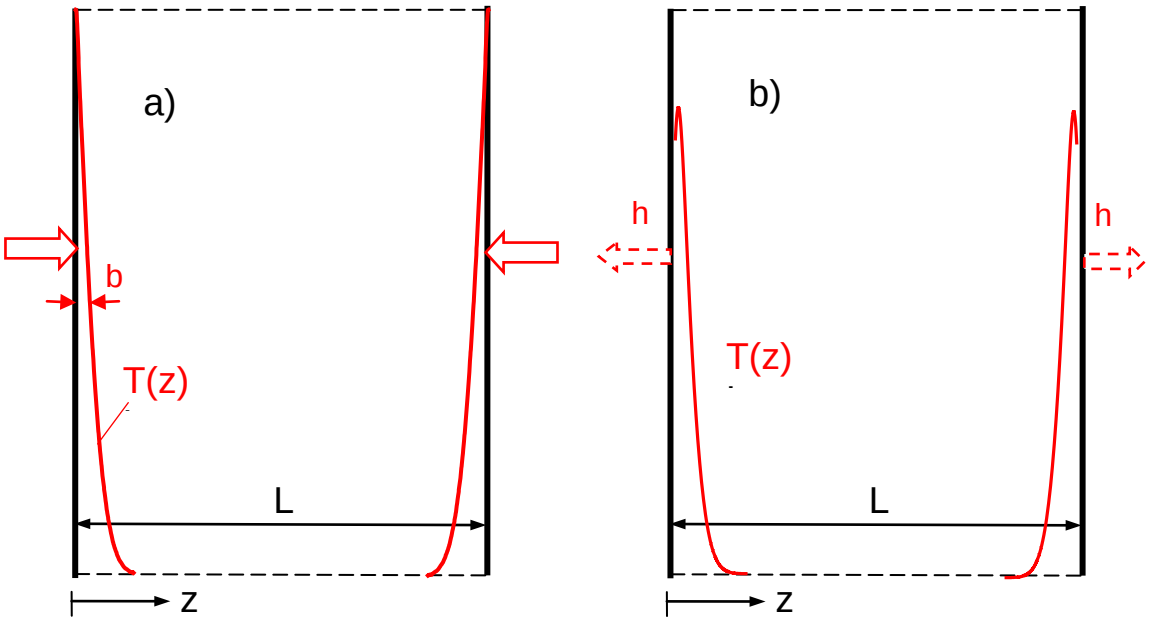

Fig. 3 a) Temperature distribution in a plate of thickness L that was heated up from the two surfaces, b) cooling down by heat radiation with heat transfer coefficient h.

This plate is then cooled down by heat radiation with the heat transfer coefficient h at the surface, shown by the red curves in Fig. 3b. The temperature after the cooling time t is given in Section 3.9 of the handbook by Carslaw and Jaeger [10]

$$T = 2\sum_{n=1}^{\infty} \exp[-\kappa\alpha_n^2 t]\frac{\alpha_n \cos\alpha_n z + h\sin\alpha_n z}{(\alpha_n^2 + h^2)L + 2h}\int_0^L T(z')(\alpha_n \cos\alpha_n z' + h\sin\alpha_n z')dz' \qquad (7)$$

where the α_n are the roots of the equation

$$\tan\alpha L = 2\frac{\alpha h}{\alpha^2 - h^2} \qquad (8a)$$

The related equation for water diffusion is then

$$C_w = 2\sum_{n=1}^{\infty} \exp[-D\alpha_n^2 t]\frac{\alpha_n \cos\alpha_n z + h/D\sin\alpha_n z}{(\alpha_n^2 + h^2/D^2)L + 2h/D}\int_0^L C_w(z')(\alpha_n \cos\alpha_n z' + h/D\sin\alpha_n z')dz' \qquad (9)$$

$$\tan\alpha L = 2\frac{\alpha(h/D)}{\alpha^2 - (h/D)^2} \qquad (8b)$$

where now C_w is the water concentration, D the diffusivity, and h stands for the mass transfer coefficient. The sum in (9) has to be taken over an infinite number of terms. This is of course hardly possible and therefore the series is replaced by finitely many terms N. First, we have to examine how large N should be at least. From eq.(9) we see, that the concentration C must reproduce the initial concentration for t=0.

2.2 Convergence behaviour

Figure 4a shows the results of eq.(9) for t=0 and N=25 (red curve) and N=200 (blue curve). Figure 4b shows three distributions for N=25, 50, and 200.

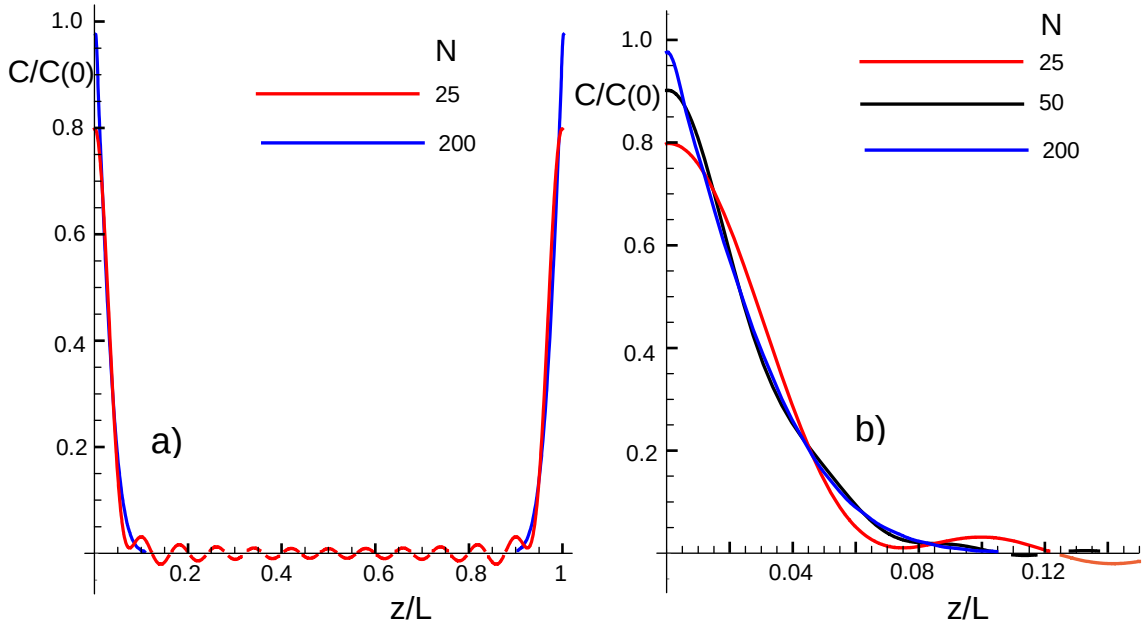

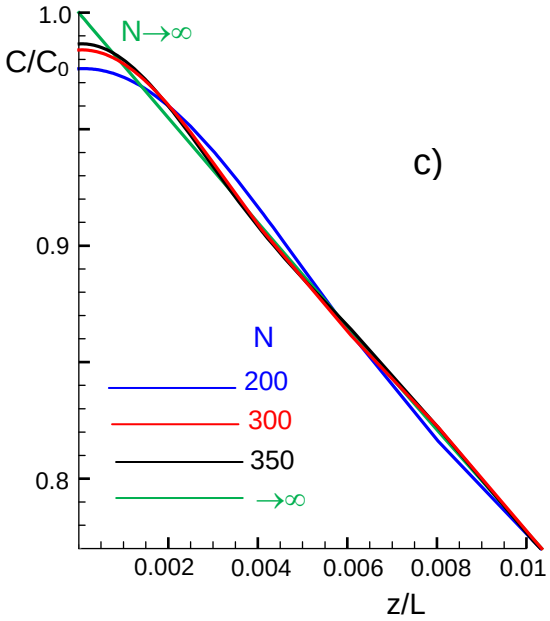

Fig. 4 Convergence of the infinite series in Eq.(9) for b/L=0.025, a) comparison of N=25 and N=200 over the whole plate, b) distributions for N=25, 50 and 200 near the surface z=0, c) distribution for N=200, 300, 350, and ∞ (close to z=0).

Finally, the curves for N=200 and N=300 are compared in Fig. 4c with the initial distribution (green curve) that corresponds to the limit $N\rightarrow\infty$. The maximum deviation of the solution with N=200 occurs at z=0 and is less 2.5%. For N=300 the deviations are less than 1.6% and can be neglected. This is the reason why we suggest solutions with 200-300 terms for further investigations.

2.3 Influence of mass transfer coefficient and time after soaking

In the calculations in Section 2.2, the case t=0 was considered. In the following calculations, the dependence of the water profiles on the time after the water uptake process is considered and the influence of the mass transfer coefficient is shown.

Figure 5 shows the effect of time t on the water profiles for hL/D=30 (Fig. 5a) and hL/D=100 (Fig. 5b). It is evident that the concentration decreases strongly with increasing time Dt/L^2 at the surface and increases in deeper zones.

Increasing mass transfer coefficient h also increases the effect of water reduction at the surface. The curves in Fig. 6a and 6b again represent the effect of mass transfer coefficient h, diffusivity D and time *t after* soaking.

Finally, Fig. 6c gives a comparison of the data measured at room temperature with the computations for $h\times L/D$=100 and $D\times t/L^2=3\times10^{-4}$. Even without the use of special fit procedures, the result is quite usable. This illustration is intended solely to show that the back diffusion of a sample into the surrounding vacuum can explain the water profiles occurring.

The results in Fig. 6c should not be understood as a curve fit, as some points could not be taken into account here, such as the influence of swelling stresses on concentration and diffusion constant.

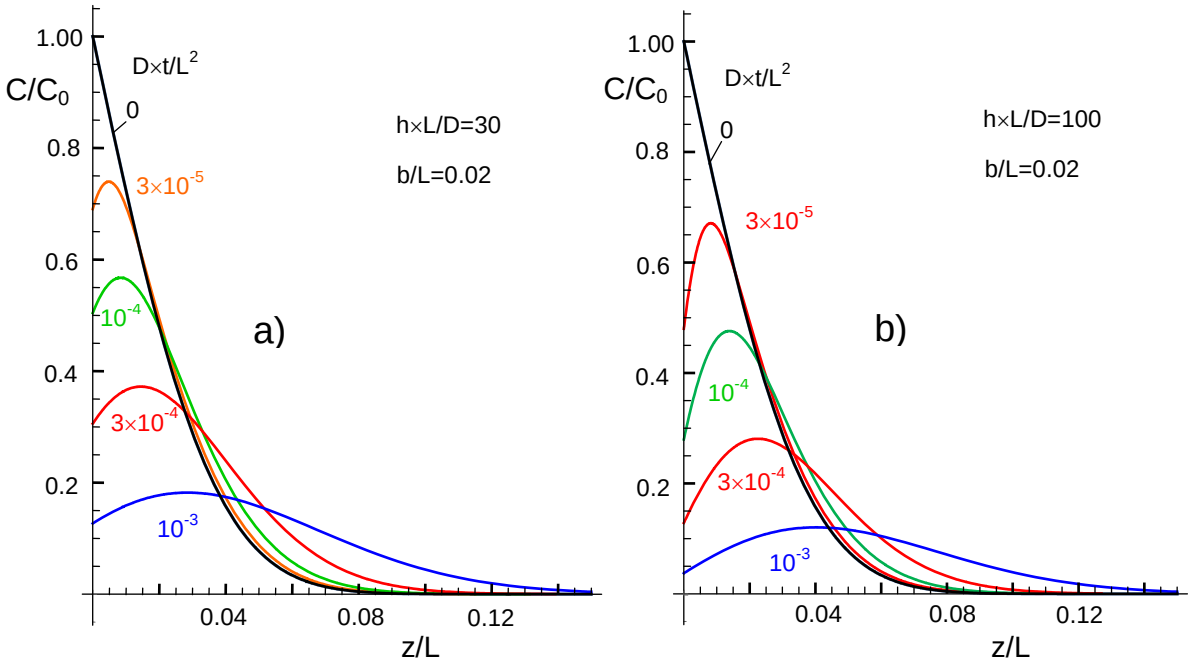

Fig. 5 Time dependence of water profiles for a) *hL*/*D*=30 and b) *hL*/*D*=100.

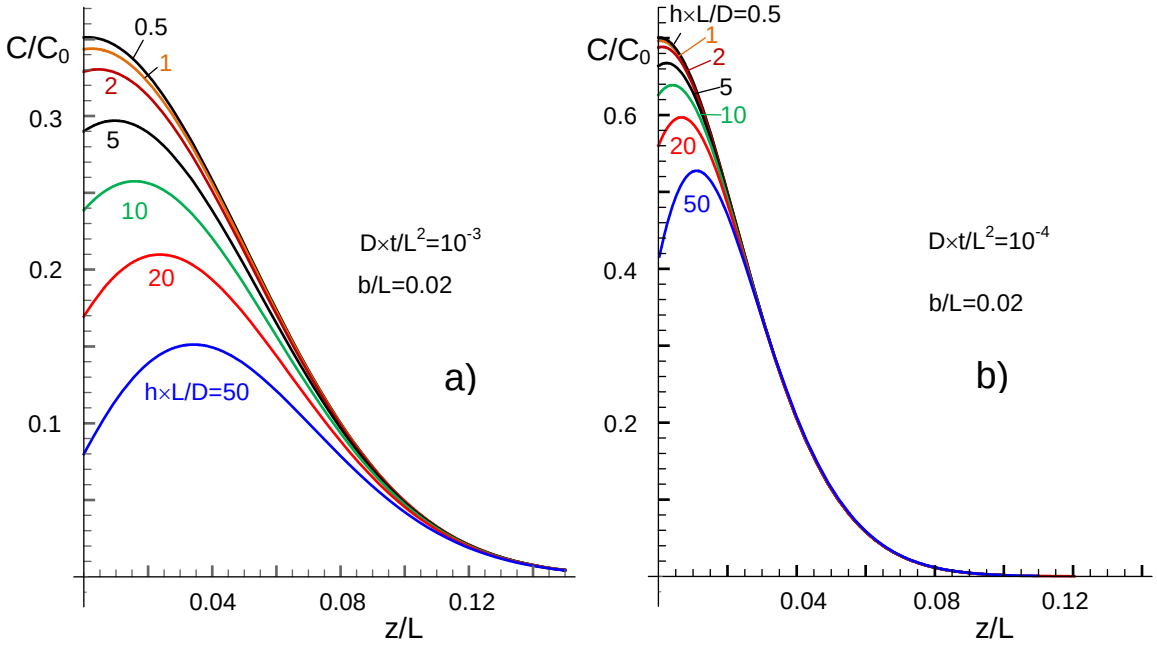

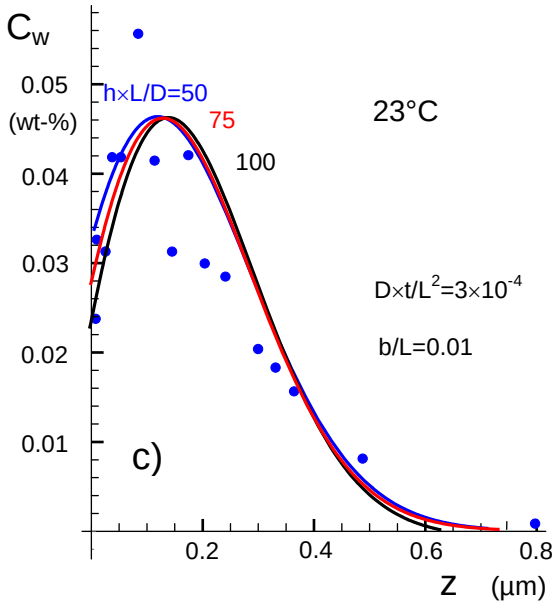

Fig. 6 Effect of mass transfer coefficient hL/D for a) $Dt/L^2=10^{-3}$ and b) $Dt/L^2=10^{-4}$, c) computed concentration profiles compared with measurements from Fig. 2c.

3 Interaction of diffusion and dissolution at silica surfaces

A further reason for deviations of the water distribution in the surface diffusion zone from an erfc-shape is caused by the dissolution of the surface material in water and a surface removal. As the glass dissolves in water, the glass/water-interface moves in the direction of diffusion. This must result in a deviation of the water concentration profile from the pure erfc law eq.(1), which was derived for a fixed glass surface.

Water concentrations C_0, expressed in hydrogen content, are shown in Fig. 7a versus temperature. For a few temperatures, Zouine et al. [1] performed multiple measurements for different soaking times. For each of these temperatures, the H-concentrations were normalized on their averages $\overline{H}$ and plotted in Fig. 7b as functions of soaking time t. From these results, we can conclude that the concentration decreases with increasing soaking time by about 5-15%. At first glance, this is a completely unexpected result.

Dissolution rates D_{dis} are plotted in Fig. 8a. The circles correspond to a soda-lime glass that should have the same dissolution behavior as silica [11]. The square shows the rate for silica at 150°C in a 0.0167 M $CaCl_2$ solution. Table 2 compiles experimental data. In our opinion, the strange soaking behavior is caused by the interaction of diffusion with dissolution of the surface material. The dissolution of the glass in water on the surface and the simultaneous diffusion of water into the glass lead to a diffusion problem with a moving diffusion source showing a correspondingly high mathematical effort, as can be seen, for example, from the work by Danckwerts [9], Masters [12], Carslaw and Jaeger [10] (Section 11), Crank [13] (Section 13), and Babich [14].

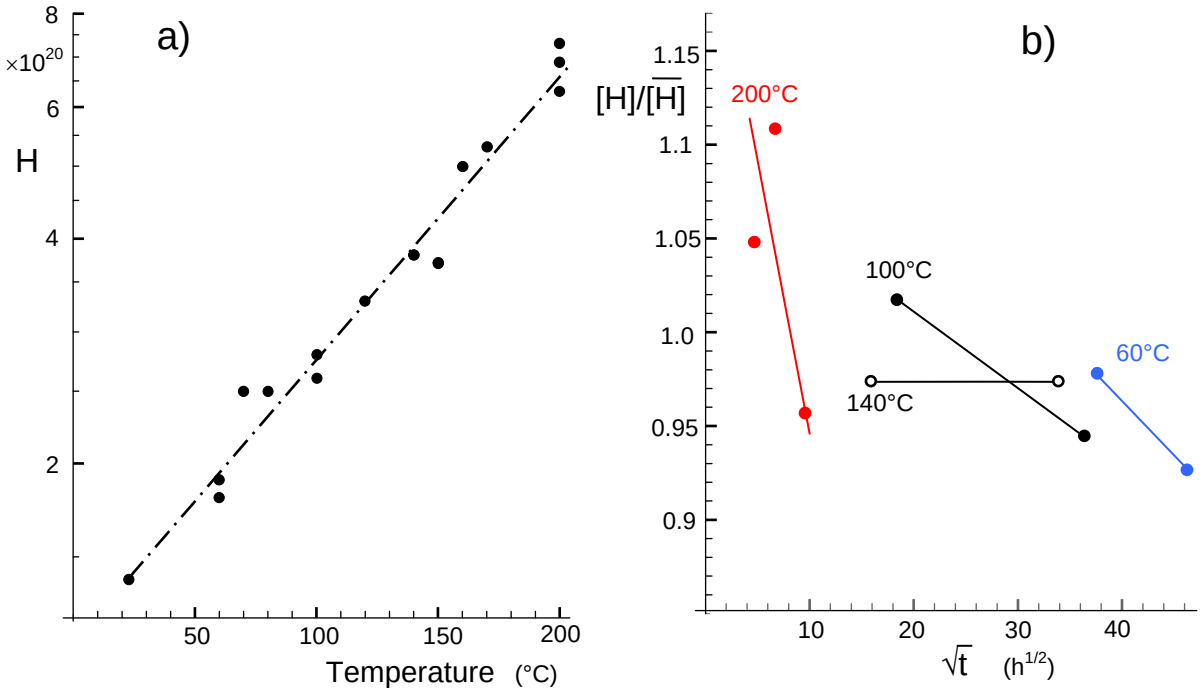

Fig. 7 a) Water concentration at a silica surface expressed in terms of hydrogen concentration H per cm^3 from Zouine et al. [1], b) results of multiple measurements by Zouine et al. [1], normalized on their averages.

Temperature	t (h)	C (10^{20} H/cm^3)	$D_{dis} \propto k$ (m/s)	D (m^2/s)
60°C	1416	1.9	3×10^{-14}	2.9×10^{-20}
	2136	1.8		3.4×10^{-20}
100°C	336	2.8	8×10^{-13}	2.9×10^{-19}
	1319	2.6		3.7×10^{-19}
140°C	253	3.8	1×10^{-11}	5.8×10^{-18}
	1147	3.8		1×10^{-17}
200°C	22	6.9	1.5×10^{-10}	7.7×10^{-17}
	45	7.3		8.5×10^{-17}
	92.5	6.3		6.0×10^{-17}

Table 2 Results from experimental data reported by Zouine et al. [1].

For a description of the behavior of real silica materials, one needs the maximum concentration at the surface $z\rightarrow0$, C_0, the dissolution rate D_{dis} and the diffusion constant D. These parameters are shown in Fig. 7a and Fig. 8a and 8b. For the case that the boundary moves in diffusion direction, the diffusion differential equation was solved by Danckwerts [9] assuming the dissolution of a solid into a supernatant liquid

$$\frac{C}{C_0} = \tfrac{1}{2}\exp[-z\sqrt{k/D}]\times \mathrm{erfc}[z/2b - \sqrt{kt}] + \tfrac{1}{2}\exp[z\sqrt{k/D}]\times \mathrm{erfc}[z/2b + \sqrt{kt}] \qquad (10)$$

where k is the velocity constant of the surface reaction between solute and solid. As indicated in Table 2, it can be assumed that k is proportional to the dissolution rate D_{dis} of Fig. 8a. The zone thickness b is defined by

$$b = \sqrt{Dt} \qquad (11)$$

For large $k\times t$, the relation (10) tends to the stationary profile

$$\frac{C}{C_0} = \exp[-z\sqrt{k/D}] \qquad (12)$$

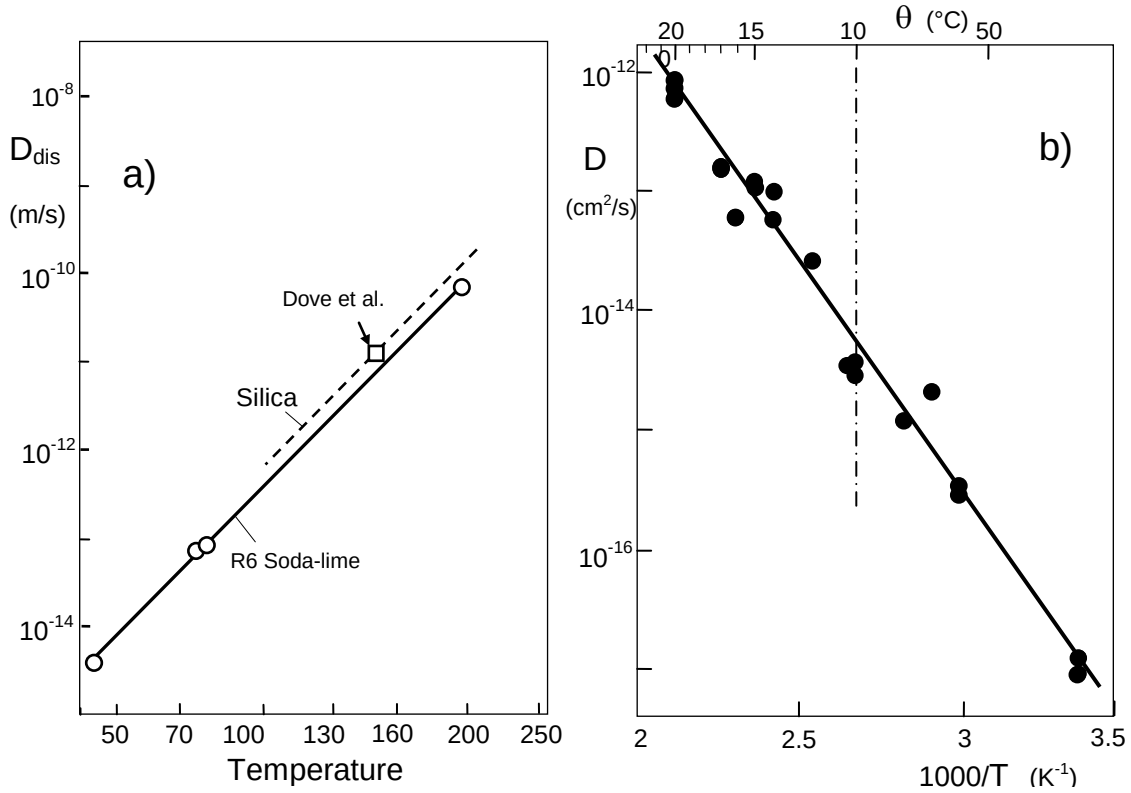

Fig. 8 a) Rate for dissolution of silica in water (circles: data for soda-lime glass R6 with about equal dissolution behaviour as silica, reported by Perera and Doremus [11], square: result from Dove et al. [15]), b) diffusivity from Zouine et al. [1].

Equation (10) is plotted in Fig. 9a for varying dissolution rates. The red curve shows eq.(1), i.e. the water profile in the absence of any dissolution. It is easy to see that the dissolution of the surface leads to strongly deviating "irregular" diffusion profiles. A comparison of eq.(10) given by the solid lines, with the stationary solution, eq.(12), represented by the dashed curves, is shown in Fig 9b. For large values of $k\times t$ the differences disappear sufficiently and eq.(12) may be used. Finally, we tried to express the curves of Fig. 9a approximately by erfc-functions modified according to

$$C \cong \alpha C_0 \operatorname{erfc}\left[\frac{z}{2\beta b}\right] \tag{13}$$

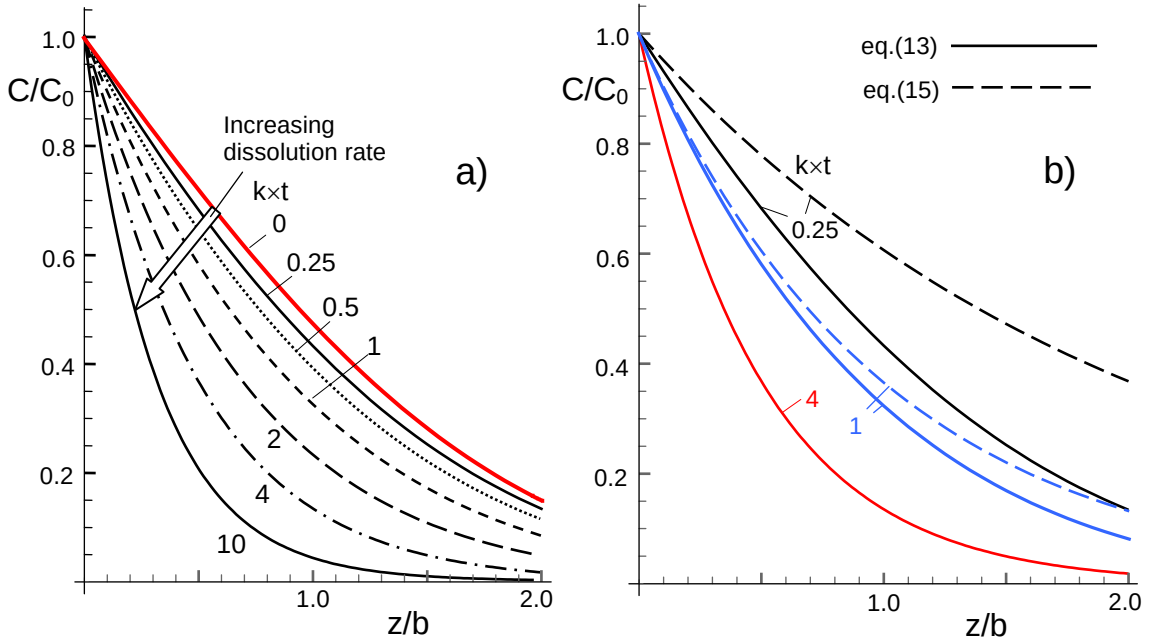

Fig. 9 Diffusion profiles affected by surface dissolution, a) Variation of profiles with the dissolution rate, b) comparison of eq.(10), solid lines, with the stationary solution, eq.(12), represented by the dashed curves. For larger $k\times t$, the two solutions can no longer be distinguished.

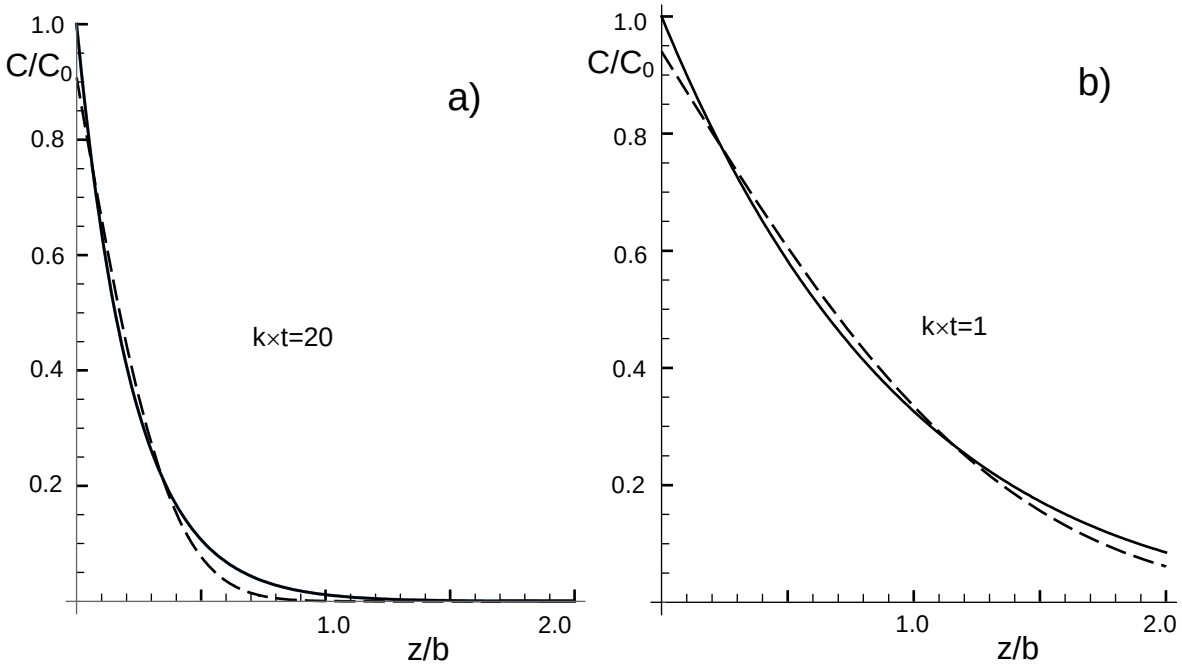

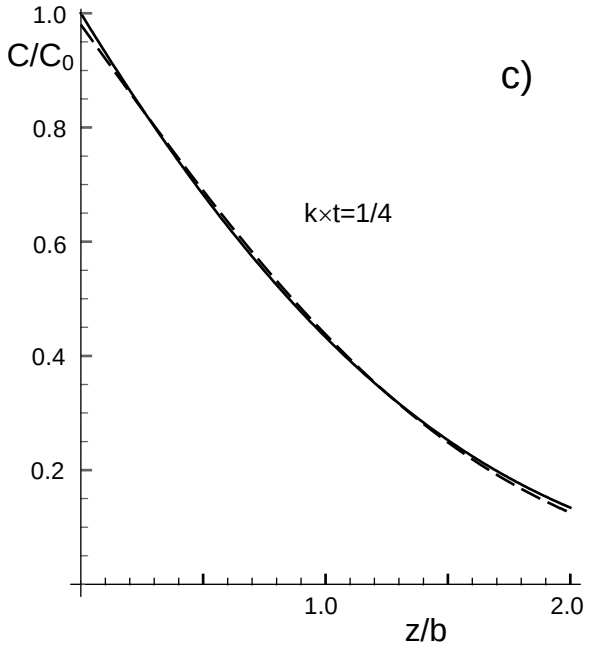

Fig. 10 Fit of some curves of Fig. 9a by an erfc-function.

The "best" set of parameters α and β was determined by application of curve fitting in the region $z/b \leq 2$ using equidistant data points. Figure 10 shows some original curves as the continuous lines together with the fitted curves (dashed lines). It can be seen, that the surface concentrations of the fitted curves are reduced by about 5-10%. The obtained parameters α and β are illustrated in Fig. 11. From Figs. 9a and 11 it becomes evident that the effect of dissolution is stronger on the shape parameter β of the erfc-representation by approximation eq.(13).

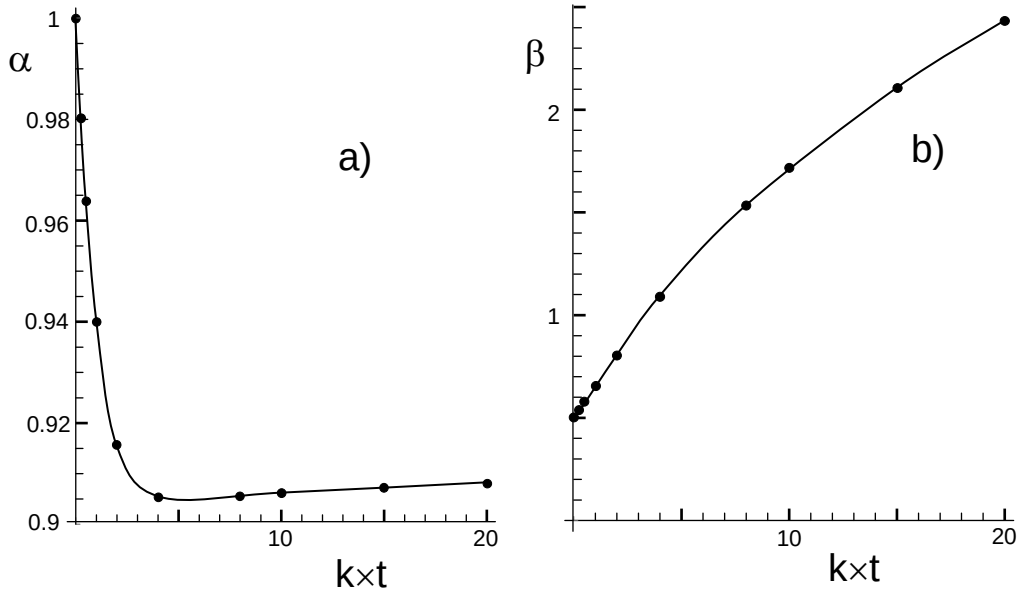

Fig. 11 Parameters for eq.(13) applied on the curves in Fig. 9a.

On the basis of the results by Zouine et al. [1] we can say that the moving boundary has a small effect of about <10% on the apparent surface concentration but a strong influence on the shape of the water profiles.

References

1 A. Zouine, O. Dersch, G. Walter and F. Rauch, "Diffusivity and solubility of water in silica glass in the temperature range 23-200°C," *Phys. Chem. Glass: Eur. J. Glass Sci and Tech. Pt. B*, **48** [2] 85-91 (2007).

2 T. Fett, G. Rizzi, K.G. Schell, C.E. Bucharsky, P. Hettich, S. Wagner, M. J. Hoffmann, Consequences of hydroxyl generation by the silica/water reaction Part I: Diffusion and Swelling, KIT Scientific Publishing, **101**(2022), Karlsruhe.

3 T. Fett, G. Schell, C. Bucharsky, Mass transfer coefficients for water at silica surfaces evaluated on the basis of literature data, **200**, 2022, ISSN: 2194-1629, Karlsruhe, KIT.

4 Oehler, A., Tomozawa, M., Water diffusion into silica glass at a low temperature under high water vapor pressure, J. Non-Cryst. Sol. **347** (2004) 211-219.

5 S. M. Wiederhorn, G. Rizzi, G. Schell, S. Wagner, M. J. Hoffmann, T. Fett, Diffusion of water in silica: Influence of moderate stresses, J. Am. Ceram. Soc. **101** (2015), 1180-1190.

6 G. T. Beilby, *Aggregation and Flow of Solids* (1921).

7 T. Fett, G. Schell, C. Bucharsky, Distribution of equilibrium constant *k* and hydroxyl *S* in silica surface layers, SWP **195**, 2022, ISSN: 2194-1629, Karlsruhe, KIT.

8 K.G. Schell, C.E. Bucharsky, T. Fett, Evaluation of water profiles at silica surfaces at 23°C, 100°C and 200°C by Zouine et al., SWP **209**, 2023, ISSN: 2194-1629, Karlsruhe, KIT.

9 P.V. Danckwerts, Absorption by simultaneous diffusion and chemical reaction, Transactions of the Faraday Society, **46**(1950), 300-304.

10 H.S. Carslaw, J.C. Jaeger, Conduction of Heat in Solids, Oxford University Press, London 1947.

11 G. Perera, R.H. Doremus, Dissolution rate of silicate glasses in water at pH 7, J. Am. Ceram. Soc. **74** (1991), 1269-74.

12 J.I. Masters, Problem of Intense surface heating of a slab accompanied by change of phase, J. Appl. Physics 17(1956) 477-484

13 J. Crank, The Mathematics of Diffusion, Clarendon Press Oxford, 1975.

14 Babich, V.M., On asymptotic solutions of the problems of moving sources of diffusion and oscillations, UDC 534.231.1, 517.226, 1991, pp. 3067-3071, Plenum Publishing Corp.

15 P.M. Dove, N. Han, A.F. Wallace, J.J. De Yoreo, Kinetics of amorphous silica dissolution and the paradox of the silica polymorphs, PNAS, **105**, [29] (2008), 9903-9908.

KIT Scientific Working Papers
ISSN 2194-1629

www.kit.edu